

Molecular BioSystems

Accepted Manuscript



This is an *Accepted Manuscript*, which has been through the Royal Society of Chemistry peer review process and has been accepted for publication.

Accepted Manuscripts are published online shortly after acceptance, before technical editing, formatting and proof reading. Using this free service, authors can make their results available to the community, in citable form, before we publish the edited article. We will replace this *Accepted Manuscript* with the edited and formatted *Advance Article* as soon as it is available.

You can find more information about *Accepted Manuscripts* in the [Information for Authors](#).

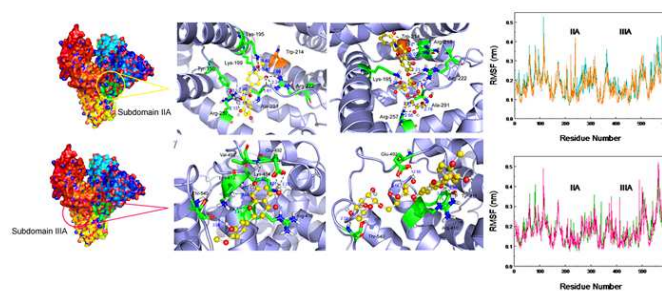
Please note that technical editing may introduce minor changes to the text and/or graphics, which may alter content. The journal's standard [Terms & Conditions](#) and the [Ethical guidelines](#) still apply. In no event shall the Royal Society of Chemistry be held responsible for any errors or omissions in this *Accepted Manuscript* or any consequences arising from the use of any information it contains.



www.rsc.org/molecularbiosystems

Graphic for Table of Contents

The biomolecular recognitions of typical flavanones, namely hesperidin and its aglycone hesperetin by critical protein have significant disparities, and these recognition distinctions may largely be originated from the flexibility of protein structure and the structural characters of bioactive flavanones.



Biological Activity of Natural Flavonoids as Impacted by Protein Flexibility: An

Example of Flavanones

Fei Ding^{acd} and Wei Peng^{*ab}

^a *College of Agriculture and Plant Protection, Qingdao Agricultural University,*

Qingdao 266109, China

^b *College of Food Science and Engineering, Qingdao Agricultural University,*

Qingdao 266109, China

^c *Department of Chemistry, China Agricultural University, Beijing 100193, China*

^d *Department of Biological Engineering, Massachusetts Institute of Technology,*

Cambridge, MA 02139, United States

*Corresponding Author

Phone/fax: +86-29-87092367

E-mail: weipeng@cau.edu.cn, wpeng@qau.edu.cn

ABSTRACT

Naturally multifunctional *Rutaceae* hesperidin and its aglycone hesperetin have a great variety of biopharmaceutical activities, e.g. anti-cancer, anti-inflammatory, antioxidant and antitumor; however, the influences of the molecular structures of hesperidin and hesperetin, and in particular, the structural properties such as flexibility and dynamic features of protein to the biological activities of these bioactive compounds remains ambiguous. In the present study, the biomolecular recognition of crucial biopolymer – albumin from human serum (HSA) with *Rutaceae*, the recognition differences between HSA-hesperidin and HSA-hesperetin, the key elements that lead to the discrepancies as well as the structural characters of protein to the recognition processes were comparatively examined by employing biophysical approaches at the molecular scale. The results illustrated distinctly that (1) aglycone hesperetin can form stronger noncovalent bonds with HSA and possess higher recognition stability as compared with hesperidin. This phenomenon suggest that the introduction of glycoside structure in flavanone may possibly not be able to increase the noncovalent recognition of flavanone by biopolymer, and conversely, this event will probably decrease the recognition capacity. (2) Although hesperidin and hesperetin can be located within subdomains IIA and IIIA, respectively, the conformational stability of flavanones in subdomain IIA is greater than subdomain IIIA; as a result, the recognition ability of subdomain IIIA with flavanones is patently lesser than subdomain IIA. These discrepancies are likely originated from the unique

characters of respective cavity, or more specifically, subdomain IIA is basically a closed space, whereas subdomain IIIA is a semi-open region. Meanwhile, the detailed analyses of Root-Mean-Square Fluctuation interpreted the recognition of flavanones by subdomain IIA on HSA would evoke larger conformational alterations in several amino acid residues, and the similar phenomenon also resides in subdomain IIIA, which signifies that the flexible characteristics of different binding patches in protein may possess fairly notable effects on the HSA-flavanones recognition. Moreover, the integrally structural changes of HSA exists some disparities on account of the dissimilarities of recognition capability to the protein-flavanones biointeractions, and all these conclusions received further forceful supports from fluorescence and circular dichroism experiments in solution. Perhaps the work emerged herein could not only help us to better evaluate the bioavailability of natural flavanones with or without glycoside, but to understand the sketches of three-dimensional structure trait of certain biomacromolecules for the medicinal properties of flavonoids in the human body.

KEYWORDS: *medicinal activity, flavanone, protein flexibility, biomolecular recognition, molecular dynamics simulation, fluorescence*

Introduction

Historically, naturally occurring bioactive compounds have always been a major medicinal source for the prevention and treatment of various human diseases. Within these crude products, flavonoids are, undoubtedly, a class of interesting agents with the most potentially applications.¹ For example, the pathological mechanisms and physiological behaviors of the human body and different free radicals are closely coupled, however, flavonoids would have excellent efficacy in preventing strong oxidation of free radicals.² Because of their numerous biological activities and medicinal values, the research of flavonoids can clearly help to treat a variety of illnesses, and thereby has great significance for the human health.^{3,4}

Flavanone comprise the majority of flavonoids in *Citrus* (Rutaceae), and it is estimated that about 95% of the flavanones comes from *Citrus* fruits such as sweet (*Citrus sinensis*) and sour oranges (*Citrus aurantium*), lemons (*Citrus limon*) and their near relatives - tangerines (*Citrus tangerina*), mandarins (*Citrus reticulata*), tangors (*Citrus reticulata sinensis*) and tangelos (*Citrus tangelo*).⁵ Through extraction and analysis of flavanones in these fruits, one may find evidently that hesperidin, (2*S*)-5-hydroxy-2-(3-hydroxy-4-methoxyphenyl)-4-oxo-3,4-dihydro-2*H*-chromen-7-yl 6-*O*-(6-deoxy- α -L-mannopyranosyl)- β -D-glucopyranoside (structure shown in Fig. 1), is the most abundant natural flavanone and the second is naringin.⁶

Fig. 1 here about

Basically, the biological activities of hesperidin have been questioned for a

relatively long time since Rusznyák and Szent-Györgyi⁷ discovered its function on capillary fragility related to scurvy in 1937. In a more recent study, Kawaguchi et al.,⁸ using an animal model, reported that hesperidin has prophylactic and curative functions on the development of collagen-induced arthritis, this chemical could thus be efficacious for treating patients with rheumatoid arthritis. Adult male Swiss mice and male Wistar rats were administered hesperidin by the routes of intraperitoneal and oral and subcutaneous injection, Loscalzo et al.⁹ found that the compound displayed depressant activity on the locomotor and exploratory effects, and exercised antinociceptive actions, whereas hesperidin failed to directly trigger off μ -opioid receptor or elicit any alteration on inward GIRK1/2 currents. Later, Elavarasan et al.¹⁰ conducted an *in vivo* experiment with young and aged male Wistar rats to investigate the potential cardioprotective effects of hesperidin. The results show unmistakably that the flavanone can boost the expression of antioxidative enzymes in aged rats and the antioxidation of hesperidin may be developed as an anti-aging medicine for humans. Furthermore, other pharmacological activities such as anticarcinogenic, antifertility, antihypertensive, anti-inflammatory, antimicrobial, cardiovascular protection, cholesterol-lowering activity, neuroprotective, and platelet and cell aggregation inhibition have also been proved in the literature.¹¹⁻¹⁷ Consequently, hesperidin is widely used in the clinical treatment of many diseases, and it is also served as raw ingredient for different drugs in pharmaceutical industry. For instance, the main raw material of the drug – Maxhoton, which is produced by the Germany Warsaw Pharmaceutical Co. Ltd., is flavanone hesperidin. Unfortunately, clinical

pharmacology demonstrate distinctly that the bioavailability of hesperidin is low (< 25%),¹⁸ and the possible reason may be attributed to the properties of the molecular structure, e.g. molecular size, polarity and steric effects. These characteristics led to the hydrolyzation of the hesperidin quickly by the gut microflora in the human body and formation of the corresponding aglycone termed hesperetin, which has also been confirmed to be active against blood lipids, inflammations, tumors, etc.^{5,6,19,20}

According to the opinion of Kroon et al.,²¹ blood is the only path for human body to contact flavonoids, on this account, these natural agents can arrive at specific location and exert their biological activities. Essentially, either pharmacological or toxicological responses will be occurred, the ligand must firstly recognize by some important biomacromolecule, and then act on the target. The feature of the noncovalent reaction would immensely regulate the physiological actions such as absorption, distribution, metabolism, excretion and toxicity of ligand in the human body. In a relatively recent study, Dangles et al.²² verified that flavonoids chiefly complexed with plasma proteins, particularly albumin from human serum (HSA), and the bioavailability of flavonoids depends largely on the HSA-flavonoids conjugates. This result coincides well with the ideas held by Yamamoto et al.²³ very recently.

Physiologically, HSA is the most plentiful plasma protein (42 g L⁻¹), where it is responsible for roughly 80% of the colloidal osmotic pressure. Like most of the plasma proteins, HSA is synthesized in the liver with a rate of nearly 0.7 mg h⁻¹ for every gram of liver (i.e. 10~15 g per day).²⁴ As a multifunctional biopolymer, HSA plays a crucial role in several physiological processes, e.g. anticoagulation, free

radical scavenging, inhibition of platelet aggregation, and deposition and transportation of many endogenous and exogenous compounds.²⁴⁻²⁶ Therefore, HSA affects the renal clearance kinetics of bound low molecular weight ligands, as binding to HSA remarkably decreases the filtration rate of these chemicals in the kidney. In addition, Davies et al.²⁷ claimed that HSA has anti-inflammatory, antioxidative and metabolic functions, so the probability that HSA will evolve as a therapeutic agent is high. Excitingly, the atomic resolution X-ray diffraction of HSA was solved by He and Carter²⁸ in 1992. It is a non-glycosylated protein of 585 amino acids (66.5 kDa), constituted of structurally homologous domains (I, II, and III) that assemble to form a heart-shaped molecule (structure shown in Fig. 2). Each domain in reverse is the product of two subdomains (A and B), which are principally helical and extensively cross-linked through 17 disulfide bridges. In general, disulfide bond contributes to the stability of HSA in the circulation, and a sole tryptophan (Trp-214) residue appears in long loop 4. The foremost cavities of ligand binding to HSA are located in subdomain IIA and IIIA, which accords wonderful with site I and site II epitomized by Sudlow et al.²⁹ in a very early study. Latest experiments by Zsila³⁰ considered that subdomain IB is the third pivotal binding patch for ligands on HSA. Structurally, several loop structures of the protein could have relatively prominent impact on the molecular recognition between HSA and diverse ligands.

Fig. 2 here about

It is generally known that proteins are the principal executants of different biological activities in the human body, thereby understanding how to run its function

in physiological processes can not only help to realize the essence of life activities, but also to become the basic premise of sickness therapy and drug design. Actually, the physicochemical properties of proteins, especially the flexibility and conformational dynamics of three-dimensional structure, are the key to comprehend their functions.^{31,32} As noted earlier, flavonoids primarily conjugated with HSA, accordingly the clarification of the information such as recognition ability and concrete domain regarding the noncovalent HSA-flavonoids possess importantly influences on grasping the pharmacokinetics of flavonoids. Results from some studies are illustrated the affinity and binding region of certain of flavonoids to HSA.³³⁻³⁵ In our previous examination, the recognition reaction of hesperidin with HSA has been probed rudimentarily,³⁶ but the effects of flexibility of the protein for the HSA-hesperidin remain obscure. And further, proteins in physiological environments undergo different conformational alterations that permit them to perform catalysis and metabolism, ligand recognition, signal transduction and so forth. However, the dynamic behavior of the HSA-hesperidin recognition is still unclear. Similarly, the flexibility and motion of HSA for the hydrolyzate of hesperidin – hesperetin (structure shown in Figure 1) recognition process are yet unresolved.

The main object of this story was to comparatively discuss the molecular recognition processes of hesperidin and hesperetin by HSA, most notably the dynamically conformational changes to respective binding region of hesperidin and hesperetin in protein based on the computer-aided molecular docking, molecular dynamics (MD) simulation as well as factually wet experiments. By expatiating the

data of MD simulation, the impacts on HSA flexibility induced by noncovalent biointeraction with two flavanones were uncovered and simultaneously, the conformational stabilities and special disparities of several critical amino acid residues which belong to the binding pocket of hesperidin and hesperetin in the molecular recognition were also disclosed in great detail. And then the outcomes of molecular modeling to the HSA-flavanones will be substantiated in solution experiments with the aid of molecular spectroscopy. These information would not only assist to further scrutinize the pharmacological properties of hesperidin and hesperetin, but shed light on the development of novel flavanones so as to raise bioavailability in the human body.

Experimental

Materials

Albumin from human serum (A3782, lyophilized powder, fatty acid free, globulin free, $\geq 99\%$, CAS number 70024-90-7), hesperidin (H5254, $\geq 80\%$, CAS number 520-26-3), hesperetin (51864, $\geq 98.0\%$, CAS number 69097-99-0), diazepam (D0899, CAS number 439-14-5), digitoxin (D5878, $\geq 92.0\%$, CAS number 71-63-6), hemin (H9039, $\geq 90\%$, CAS number 16009-13-5) and warfarin (A2250, CAS number 81-81-2) were purchased from Sigma-Aldrich (St. Louis, MO) and used without further purification, and deionized water was generated by a Milli-Q

Ultrapure Water Purification Systems from Millipore (Billerica, MA). Tris (0.2 M)-HCl (0.1 M) buffer of pH=7.4, with an ionic strength 0.1 in the presence of NaCl, and the pH was checked with an Orion Star A211 pH Benchtop Meter (Thermo Scientific, Waltham, MA). Dilutions of the HSA stock solution (10 μ M) in Tris-HCl buffer were prepared immediately before use, and the concentration of protein was measured by the method of Lowry et al.³⁷ All other reagents employed were of analytical grade and received from Sigma-Aldrich.

Molecular docking

Molecular docking of the HSA-flavanone adducts was operated on SGI Fuel Visual Workstation. The crystal structure of HSA (entry codes 1H9Z),³⁸ determined at a resolution 2.5 Å, was retrieved from the Brookhaven Protein Data Bank (<http://www.rcsb.org/pdb>). After being imported in the program Sybyl Version 7.3 (<http://www.certara.com>), HSA structure was carefully checked for atom and bond type correctness assignment. Hydrogen atoms were computationally added using the Sybyl Biopolymer and Build/Edit menus. To avoid negative acid/acid interactions and repulsive steric clashes, added hydrogen atoms were energy minimized with the Powell algorithm with 0.05 kcal mol⁻¹ energy gradient convergence criteria for 1500 cycles, this procedure does not change positions to heavy atoms, and the potential of the three-dimensional structure of HSA was assigned according to the AMBER force field with Kollman all-atom charges. The two-dimensional structures of flavanones

were downloaded from PubChem (<http://pubchem.ncbi.nlm.nih.gov>), and the initial structures of these molecules were produced by Sybyl 7.3. The geometries of flavanones were subsequently optimized to minimal energy (tolerance of 0.5 kcal mol⁻¹) using the Tripos force field with Gasteiger-Hückel charges, and the lowest energy conformer was utilized for the docking analysis. The Surflex-Dock program which employs an automatic flexible docking algorithm was applied to analyze the possible conformations of these ligands that bind to HSA, and the program PyMOL (<http://www.pymol.org>) was finally used for visualization of the molecular docking results.

Molecular dynamics simulation

Molecular dynamics (MD) simulation of HSA-flavanone complexes was performed using Gromacs program,³⁹ version 4.5.5, with the Gromacs96 53a1 force field.⁴⁰ Initial conformations of HSA and flavanones were, respectively, taken from the original X-ray diffraction crystal structure that was solved at 2.5 Å resolution (entry codes 1H9Z) and the optimal structures originated from molecular docking. The topologies of HSA were generated by Gromacs package directly, whereas flavanones by PRODRG2.5 server.⁴¹ The simulation systems were solvated with a periodic cubic box (the volume is 7.335×6.155×8.119 nm³) filled with TIP3P water molecules and an approximate number (15) of sodium counterion to neutralize the charge. Totally, there are 51,206 crystallographic solvent molecules, and the shortest

distance between the complex and the edge of the box is set to 12 Å. Simulations were carried out using the isothermal-isobaric (NPT) ensemble with an isotropic pressure of 1 bar, and the temperature of the ligand, protein and solvent (water and counterion) was separately coupled to an external bath held at 298 K, using the Berendsen thermostat with 0.1 ps relaxation time.⁴² The LINCS algorithm was used to constrain bond lengths,⁴³ and the long-range electrostatic interactions beyond 10 Å were modeled using the Particle Mesh Ewald (PME) method with a grid point density of 0.1 nm and an interpolation order of 4.⁴⁴ A cutoff of 12 Å was used for van der Waals' interactions. The MD integration time step was 2.0 fs and covalent bonds were not constrained, and the system configurations were saved every 2.0 ps. To decrease the atomic collisions with each other, both gradient descent and conjugate gradient algorithm were employed to optimize the whole system. First the solvated starting structure was preceded by a 1,000-step gradient descent and then by conjugate gradient energy minimization.^{45,46} Subsequently, 500 ps equilibration with position restraints runs to remove possible unfavorable interactions between solute and solvent, and after thorough equilibration, MD simulations were run for 12 (HSA-hesperidin, subdomain IIA), 15 (HSA-hesperidin, subdomain IIIA), 8.5 (HSA-hesperetin, subdomain IIA) and 15 (HSA-hesperetin, subdomain IIIA) ns, respectively. The results of MD simulations were finally displayed by Visual Molecular Dynamics 1.9.1,⁴⁷ and the program Discovery Studio Visualization 4.0 (Accelrys, San Diego, CA) was utilized to show the images of the MD simulations.

Fluorescence emission spectra

Fluorescence spectra were obtained with a 1.0 cm path length quartz cell using a F-7000 spectrofluorimeter (Hitachi, Japan) equipped with a thermostatic bath. The excitation and emission slits were set at 5.0 nm each, intrinsic fluorescence was carried out by exciting the continuously stirred protein solution at 295 nm to favor Trp residue excitation, and the emission spectra were read in the wavelength range of 300-450 nm at a scanning speed of 240 nm min⁻¹. The reference sample consisting of the Tris-HCl buffer of flavanones in corresponding concentrations was subtracted from all fluorescence measurements.

Site-specific ligand

Binding location studies between HSA and flavanones in the presence of four typical site markers (warfarin, diazepam, digitoxin and hemin) were executed using the fluorescence titration approach. The concentration of HSA and site markers were held in equimolar (1.0 μ M), then flavanones were respectively added to the HSA-site markers mixtures. An excitation wavelength of 295 nm was chosen and the fluorescence emission wavelength was acquired from 300 to 450 nm.

Circular dichroism

Circular dichroism (CD) was collected with a Jasco-815 spectropolarimeter (Jasco, Japan) equipped with a microcomputer, the apparatus was sufficiently purged with 99.9% dry nitrogen gas before starting the instrument and then it was calibrated with d-10-camphorsulfonic acid. All the CD spectra were taken at 298 K with a PFD-425S Peltier temperature controller attached to a water bath with an accuracy of ± 0.1 °C. Each spectrum was performed with use of a precision quartz cuvette of 1.0 cm path length and taken at wavelengths between 200 and 260 nm range that provides a signal extremely sensitive to small secondary conformational distortions. Every determination was the average of five successive scans encoded with 0.1 nm step resolution and recorded at a speed of 50 nm min⁻¹ and response time of 1 s. All observed CD data were baseline subtracted for buffer and the estimation of the secondary structure elements was obtained by exploiting Jasco Spectra Manager II, which computes the different designations of secondary structures by comparison with CD spectra, determined from distinct proteins for which high-quality X-ray diffraction data are available.

Statistical analysis

All assays were executed in triplicate, the mean values, standard deviations, and statistical differences were estimated using analysis of variance (ANOVA). The mean values were compared using student's *t*-test, and all statistical data were treated using the OriginPro Software (OriginLab Corporation, Northampton, MA).

Results and discussion

Molecular modeling

In general, molecular modeling can not only consider the receptor's structural information and the interrelationships of receptor-ligand, but also reasonably deduce other important parameters such as binding mode and affinity; thereby this method has become one of the most significant techniques for the exploration of bioactive ligand-biomacromolecule noncovalent reaction, and is widely used in numerous areas, e.g. environmental toxicology, food chemistry and medicinal chemistry.⁴⁸

(I) Molecular docking

In order to probe the crucially active groups in flavanones, the key amino acid residues in protein, and the binding patterns between them, we first use molecular docking to investigate minutely the HSA-hesperidin, and then contrast this adduct with its parent compound hesperetin-HSA complex. In this way we may obtain an overall perception of the HSA-flavanone reactions. The optimal energy conformations of hesperidin and its aglycone – hesperetin in protein are shown in Fig. 3, and the concrete hydrogen bonds and its corresponding bond lengths are also listed in Table 1. Obviously, both hesperidin and hesperetin has the ability to locate within subdomains

IIA and IIIA (Fig. S1, Supporting Information), but the affinity of subdomain IIIA with flavanone is lesser than subdomain IIA. According to the binding mode patterns and Table 1, it is clear that hesperidin can make five strong hydrogen bonds with the amino acid residues such as Lys-195, Arg-222 and Arg-257 in the subdomain IIA (Fig. 3(A)), while there are still three relatively weak hydrogen bonds between hesperidin and Arg-218 and Ala-291 residues. In addition to hydrogen bonds, conjugated effect also exists in the protein-ligand system. Definitely, the plane of benzene ring (C-ring) in hesperidin is perpendicular to the plane of indole ring in Trp-214 residue, and the distance between the center of the two rings is 3.56 Å, which indicated evidently that the presence of *T*- π stacking between subdomain IIA and hesperidin. However, hesperidin may just form five hydrogen bonds with some amino acid residues, i.e. Arg-410, Tyr-411, Glu-492 and Thr-540 in subdomain IIIA (Fig. 3(B)), and the bond lengths are displayed in Table 1. Unmistakably, hesperidin could be situated stably within subdomain IIIA mainly through powerful hydrogen bonds, and there had no palpable conjugated effect between subdomain IIIA and hesperidin.

Fig. 3 here about

Table 1 here about

Similarly, the aglycone hesperetin has the capacity to yield six very strong hydrogen bonds with Arg-222, Arg-257 and Ala-291 residues in subdomain IIA on HSA (Fig. 3(C)) and, meanwhile, there are other three somewhat forceful hydrogen bonds between hesperetin and the amino acid residues Tyr-150, Lys-195 and Lys-199. Furthermore, the plane of benzene ring (B-ring) in hesperetin and the plane of pyrrole

ring in Trp-214 residue are vertical, and the distance between the core of two rings is plainly 4.12 Å, implying that T - π stacking also operated between subdomain IIA and hesperetin. Nevertheless, the intensity of T - π stacking in the HSA-hesperetin is relatively small as compared with the HSA-hesperidin complexes. Although hesperetin can be located at the subdomain IIIA on HSA (Fig. 3(D)), the situation does not completely cohere with the hesperidin in this region. Hesperetin might generate stronger hydrogen bonds with Arg-410, Glu-492 and Thr-540 residues owing to the shorter bond lengths, whereas the strength of hydrogen bonds between hesperetin and the Lys-413, Lys-414 and Val-493 residues is weak but the hydrogen bonds are still worked. Moreover, the perceptible conjugated effect does not exist between hesperetin and subdomain IIIA, which has a close resemblance to hesperidin in the same pocket. Hence, one can come at the logical conclusions from the above molecular docking that the binding magnitude of hesperidin for subdomain IIA is slightly greater than the subdomain IIIA, and the principal reason for this issue is the noncovalent interactions of hesperidin to the amino acid residues in subdomain IIA are somewhat stronger than the noncovalent bonds in subdomain IIIA. As regards HSA-hesperetin mixture, however, the reaction strength of hesperetin with subdomain IIIA is substantially smaller than the subdomain IIA on HSA.

(II) Molecular dynamics simulation

Molecular dynamics (MD) simulation is a method for exploring the

macroscopically hypostatic properties by means of microcosmic motion. Based on the Newton's laws of motion, MD simulation can extrapolate the acceleration, position, velocity, etc. of each atom at every time interval, and then analyze these data by using statistical mechanics so as to receive other pivotal parameters. Therefore, MD simulation may not only help us to further understand the importantly dynamic processes in biological systems at the atomic/molecular level, but also to explain/predict exactly the structure-function relationships of biomacromolecules in nature.^{49,50} Currently, this technique is gradually applying to many fields such as the structural modifications of nuclear magnetic resonance, X-ray analysis, the speculation of different macroscopic property and microcosmic mechanism, and it has also become an indispensable tool of our scientific research. To acquire the corroborative evidence of equilibrium state for the biopolymer-ligand and validate the rationality of molecular docking, MD simulation has been used to study the binding mode of the HSA-flavanone adducts, and the Root-Mean-Square Deviation (RMSD) of the four systems are displayed in Fig. 4. Essentially, the RMSD of protein's skeleton structure and initial structure in the MD simulation is the determination of the average distance between the atoms (usually the backbone atoms) of superimposed proteins. A system can be regarded as in equilibrium if the RMSD value fluctuates steadily within a narrow range. As shown in Fig. 4, the adducts, hesperidin (Fig. 4(A)) and hesperetin (Fig. 4(C)) in subdomain IIA, respectively, and hesperetin (Fig. 4(D)) in subdomain IIIA could reach equilibrium and stabilization in a short time, while hesperidin (Fig. 4(B)) in subdomain IIIA is very unsettled.

Fig. 4 here about

Concretely, the RMSD of the backbone C_{α} atoms of HSA (Fig. 4(A)) increased slowly and then stabilized at about 0.35 nm after $\sim 5,000$ ps MD simulation; and the hesperidin is nearly under equilibrium state (0.15 nm), at time point $\sim 10,100$ ps, a marginally rise in the RMSD of hesperidin may be detected and presently the value equilibrated at 0.175 nm until the end-point time 12,000 ps. Conversely, it is difficult for Fig. 4(B) to get dynamic equilibrium state, the RMSD of the backbone C_{α} atoms of protein gradually declined from the time 2,000 ps to 8,000 ps; and raised tardily to equilibrium state at roughly 9,000 ps. However, the RMSD of hesperidin ascended rapidly to 0.371 nm at approximately 1,245 ps, then reached the dynamic equilibrium at $\sim 6,600$ ps and the backbone RMSD is 0.17 nm. As for the HSA-hesperetin, the noncovalent systems can preserve favorable stability regardless of subdomains IIA and IIIA. It is conspicuous from Fig. 4(C) the RMSD of the backbone C_{α} atoms of HSA began to stabilize at the time point 2,000 ps, and always fluctuated at ~ 0.3 nm; the RMSD of hesperetin remained outstandingly at 0.075 nm till the simulation process is finished (8.5 ns). While the RMSD of the biopolymer started to achieve equilibrium state (0.325 nm) at the time scale 1,000 ps, and the RMSD of hesperetin oscillated patently at ~ 0.06 nm (Fig. 4(D)). Based on the foregoing analyses of RMSD values, we can legitimately find that the stability of both hesperidin and hesperetin in subdomain IIA is remarkably superior to subdomain IIIA. This fact illustrate distinctly that the affinity capability of flavanones for subdomain IIIA on HSA is lower than subdomain IIA, which further confirms the outcomes derived from

molecular docking are reliable, i.e. the noncovalent interactions of flavanones with the amino acid residues in subdomain IIA are evidently higher than the amino acid residues in subdomain IIIA. Further, compare the conformations of hesperetin in the two dominant binding patches with its glycoside – hesperidin, one could also ascertain that the stability of hesperetin notably outweigh the flavanone hesperidin.

In order to scrutinize the spatial differences of the whole protein-flavanones between the initial conformation and the optimal conformation, and check the distance changes of hydrogen bonds between the crucial amino acid residues and the average conformation in the MD simulation, the average conformation in the last 4,000 ps simulation has been selected and overlapped the initial conformation, and the superposition pictures are appeared in Fig. 5. The discrepancy in the average and initial conformations centers chiefly in the glycoside structure when the hesperidin situate within subdomain IIA (Fig. 5(A)). Apparently, the two glycosides in the hesperidin are linked by the rotatable single bond, and the glycoside structures can distort so as to near the Arg-222 residue. This feature, in a manner, strengthened the noncovalent interactions between the flavanone and the hydrogen atom of the amino group in Arg-222 residue. Simultaneously, the hydrogen bonds between hesperidin and Arg-257 residue weakened, to be specific, the bond lengths between the oxygen atom in the glycoside structure and the hydrogen atom of the amino group in Arg-257 residue had increased to 2.87 Å and 2.96 Å, respectively; whereas the hydrogen bond between hesperidin and the Ala-291 residue evidently melted away. Furthermore, because the Arg-222 residue lie in the loop 4 with large flexibility, the two hydrogen

bonds of this residue with the oxygen atom (O-1) of the tetrahydropyran ring (D-ring) and the oxygen atom between the benzene ring (A-ring) and the tetrahydropyran ring (D-ring) have been turned with the hydrogen atom of the hydroxyl group in glycoside structure, and the bond lengths are respectively 1.68 Å and 2.73 Å. Therefore, it is quite plain that the glycoside structure and the rotary single bond endow hesperidin with expandable and flexural characters in the subdomain IIA on HSA, and enhance the instability of the flavanone conformation.

Fig. 5 here about

As noted earlier, the HSA-hesperidin adduct was unstable as the flavanone located at subdomain IIIA in protein. The probable reason for this is that the reaction between subdomain IIIA and hesperidin belong to surface conjugation (Fig. 5(B)), and there are many rotatable single bonds in the hesperidin structure. As a result, the conformation would need relatively long time to reach dynamic equilibrium state, and both glycoside and parent structures in hesperidin befall displacement, thereby inducing the disappearance of hydrogen bond between the hydrogen atom of the hydroxyl group (3-OH) in tetrahydropyran ring (D-ring) and the oxygen atom of the carboxyl group in Glu-492 residue. Moreover, the hydrogen bond between the oxygen atom of the hydroxyl group (4-OH) in tetrahydropyran ring (E-ring) and the hydrogen atom of the amino group in Thr-540 residue has been abated as a result of conformational alterations, and practically the bond length has increased from 2.02 Å to 3.02 Å, hence the weak interactions of the entire noncovalent system should be lessened.

Still, the conformation of parent compound hesperetin did not alter significantly when the chemical lie inside the subdomain IIA on HSA (Fig. 5(C)), and the small changes focused principally on the single bond rotation between the benzene ring (B-ring) and the tetrahydropyran ring (C-ring), which made some hydrogen bonds to evaporate and the others to reinforce in the meantime. For example, the bond lengths of two infirm hydrogen bonds computed from molecular docking, that is the oxygen atom of the methoxy group in benzene ring (B-ring) with the hydrogen atom of the amino group in Lys-195 and Lys-199 residues, respectively, were found to be outstripped 3.50 Å after the dynamics equilibrium, which meant that the hydrogen bonds became more weaker owing to the longer bond lengths (3.42 Å and 3.40 Å) in the initial conformation. However, it is evident that the hydrogen bonds between the hesperetin and the Arg-222 residue strengthened distinctly, and the relative displacement also arose in some functional groups having weak interactions. These effects noticeably led to the reduction of bond lengths from 1.99 Å and 2.24 Å to 1.62 Å and 1.89 Å, respectively. It is worthwhile to note that both the number and the strength of hydrogen bonds for hesperetin in subdomain IIA increased in general, but there are some exceptions. For instance, the bond length between the hydrogen atom of the hydroxyl group (5'-OH) in benzene ring (B-ring) and the oxygen atom of the carbonyl group in Arg-291 residue has changed from 1.61 Å to 2.00 Å, which also falls within the ambit of the strong hydrogen bond. And, the plane of benzene ring (B-ring) and the surface of the pyrrole ring in Trp-214 residue tend to parallelism due to torsion of single bond, which promotes the $T-\pi$ stacking to transmate into $\pi-\pi$

stacking to a certain degree.

In addition, comparison with the evenly average conformation and the initial conformation of hesperetin in subdomain IIIA on HSA (Fig. 5(D)), we can lucidly detect the disappearance of the hydrogen bond between the oxygen atom of the hydroxyl group (7-OH) in benzene ring (A-ring) and the hydrogen atom of the amino group in Lys-414 residue, while the intensity of hydrogen bond between the same oxygen atom in hesperetin and the hydrogen atom of the amino group in Val-493 residue has expanded outstandingly owing to the compression of bond length from 3.42 Å to 2.24 Å. Nonetheless, the hydrogen atom of the hydroxyl group (7-OH) in benzene ring (A-ring) and the oxygen atom of the hydroxyl group (5-OH) in benzene ring (A-ring) were observed to be made two hydrogen bonds with the oxygen atom of the carbonyl group in Arg-222 and the hydrogen atom of the amino group in Arg-222 residue, and the bond lengths are 2.68 Å and 2.91 Å, respectively. The qualities of the other hydrogen bonds for the hesperetin in subdomain IIIA have also discernible changes at the same time. Consequently, one may get a conclusion from the disparity in superimposed conformation that the benzene ring (A-ring) and the tetrahydropyran ring (C-ring) of hesperetin inclines to elicit spatial displacement whereas benzene ring (B-ring) hold comparatively firm.

The Root-Mean-Square Fluctuation (RMSF) can efficiently resolve the matchable atomic position variance of the balanced conformation in MD simulation and the initial conformation to biomacromolecule, thereby inspecting the alterations of flexibility in biopolymer. To comprehensively examine the characteristics of protein

flexibility in MD simulation, the RMSF values of the four HSA-flavanone adducts have been compared and the results are exhibited in Fig. 6. It was apparent from Fig. 6(A) that the complexed state of both hesperidin and hesperetin in subdomain IIA are almost parallel, and the RMSF of the two systems overlap marvellously with the distribution of protein secondary structures. Analogously, the changes of RMSF to flavanones in subdomain IIIA can also be superposed perfectly, which interpreted the two flavanones have similar influences upon the identical subdomain in HSA and thus witnessing the accordant mechanism in the protein-flavanone biointeractions. Moreover, the fluctuations of RMSF to subdomain IB and IIIB are evident because of the larger flexibility of the two regions; on the contrary, the fluctuation range of RMSF is relatively small since the subdomains IIA and IIIA have somewhat smaller flexibility.

Fig. 6 here about

Interestingly, the RMSF of subdomain IIA (residues 199~292) complexes with flavanones is more prominent than the changes in RMSF of the subdomain IIA unfixed with flavanones. Visually, several amino acid residues in Fig. 6(A) such as Arg-222, Lys-240 and Ala-291 owns higher RMSF, but no uniform phenomena can be seen for the amino acid residues subordinated to subdomain IIA in Fig. 6(B). These facts expounded clearly the greater spatial displacement has emerged into the amino acid residues which belong to subdomain IIA as a result of protein-flavanone conjugations. As for the subdomain IIIA (residues 384~489), the amino acid residues, e.g. Lys-413 and Ala-490 can produce larger RMSF, which means that flavanones

located at subdomain IIIA could cause the generation of bigger displacement and rotation in amino acid residues, and this issue should be mostly attributed to the polar interactions between the biopolymer and the flavanones. In the light of the anatomization of RMSF regarding the HSA-flavanone systems, we may draw the conclusion that there are similar impacts on the biomacromolecule when the hesperidin and hesperetin situate within the same binding domain on protein, which also implies that the biointeractions between HSA and flavanones have parallel action mechanism. Furthermore, the noncovalent interactions of flavanones with subdomains IIA and IIIA can probably arouse major displacement and rotation in partial amino acid residues as the two subdomains possesses fairly flexible properties in the three-dimensional structure of protein.

Fluorescence spectroscopy

Fluorescence is frequently used in many fields such as chemical biology, food science and pharmaceutical research. By measuring physicochemical parameters, e.g. fluorescence intensity and lifetime, of the fluorophore in samples, this method can provide association constant, reaction mechanism, rate constant, reaction extent, conformational alterations in biopolymers, etc. to a specific reaction system.^{51,52} In order to study the reactive behavior of both hesperidin and hesperetin with HSA, fluorescence emission spectra of protein at pH=7.4 and $T=298$ K with different concentrations of flavanones following an excitation of 295 nm are displayed in Fig. 7.

Actually, HSA involve three amino acid residues that contribute to its ultraviolet fluorescence, that is Phe, Trp and Tyr, but emission of HSA is predominated by Trp residue which absorbs at the longest wavelength and shows the largest extinction coefficient. Hence, Trp residue in the protein can usually be selected as a valuable research target owing to the high sensitivity of the residue to its local environment.

Fig. 7 here about

It is very clear from Fig. 7 that HSA indicated a relatively strong fluorescence emission peak at 334 nm, and the augment of flavanones set off an arresting decrease in the fluorescence intensity of Trp residue. Moreover, the pure flavanones reveals no fluorescence emission in the range 300~450 nm under the experimental conditions, which did not interfere with the determination of HSA intrinsic fluorescence. These events prescribed undoubtedly that there were some kinds of conjugations between the biomacromolecule and the flavanones, and the two compounds really situated in the subdomain where Trp residue located within or near the single fluorophore.^{53,54} It should also be noted that the quenching effect of protein fluorescence arose by hesperetin is greater than its glycoside – hesperidin (Fig. S2), and the chief cause for the difference is the discrepancy in ligand structure and domain characteristic, which has been uncovered detailedly based on the data of molecular docking and MD simulation.

Basically, the emergence of fluorescence quenching relies on the mechanism, which in reverse rests with the chemical properties of the independent ligands, thus the exhaustive resolution of the reaction mechanism is needed for a given

fluorescence event. To check the essence of the fluorescence reactions between HSA and flavanones, the fluorescence data were processed according to the Stern-Volmer equation (2), and the corresponding outcomes derived from Stern-Volmer plot (Fig. 8) were found to be $K_{SV} = 5.04 \times 10^3 \text{ M}^{-1}$ and $k_q = 8.428 \times 10^{11} \text{ M}^{-1} \text{ s}^{-1}$ for HSA-hesperidin and $K_{SV} = 6.65 \times 10^3 \text{ M}^{-1}$ and $k_q = 1.112 \times 10^{12} \text{ M}^{-1} \text{ s}^{-1}$ for HSA-hesperetin, respectively. Intuitively, a linear Stern-Volmer plot is suggestive of a single type of fluorophores, all equally accessible to quencher. Therefore the linear relationships in Fig. 8 are symptomatic of just one fluorescence mechanism within the biological interactions of flavanones with the globular protein. It is obvious that the values of k_q are roughly 100-fold larger than the diffusion-controlled quenching constant ($1.0 \times 10^{10} \text{ M}^{-1} \text{ s}^{-1}$) in aqueous solution, which certifies that the fluorescence decrement of protein should be mainly dominated by a static type rather than a dynamic quenching.⁵⁵

Fig. 8 here about

It is also essential to notice that static and dynamic quenching may be explained by Stern-Volmer equation (2) based upon fluorescence quenching data, but the measurement of fluorescence lifetimes is the most definitive method to elaborate fluorescence quenching. In order to further illuminate the HSA-flavanones biointeractions, time-resolved fluorescence decay of protein at various molar ratios of flavanones in Tris-HCl buffer, pH=7.4, were scanned and the fluorescence lifetimes and their amplitudes are collected in Table 2. Observably, the decay curves of HSA fitted well to a biexponential function kinetics, and Table 2 clearly show that a short

lifetime $\tau_1=3.49$ ns and a long lifetime $\tau_2=6.95$ ns ($\chi^2=1.05$) for HSA during the fluorescence lifetime decay; while in the maximal concentration of flavanones, the fluorescence lifetime components are $\tau_1=2.05/2.16$ ns and $\tau_2=6.68/6.69$ ns ($\chi^2=1.11/1.03$) for hesperidin/hesperetin, respectively. The biexponential decay of HSA in the current situation could be attributed to a single electronic transition of Trp residue, which can explicate the presence of rotational conformational isomers (rotamers) in the folded structure of globular protein.^{56,57}

Table 2 here about

These rotamers have different orientations of the amino and carboxyl groups relative to the indole ring and the investigation of lone Trp residue HSA has offered information on the spectral properties of Trp residue in unique environments. In reality, owing to steric effects between the side chain of Trp residue and the backbone of polypeptide chain, all rotamers are not completely feasible. The quenching group nearest to the indole ring is the small amino group after HSA-flavanones complexes shaped, thereby the rotamer with the supreme population and the fluorescence lifetime of 6.95 ns. Conversely, if amino and carbonyl group near the indole part, this rotamer may possess the short fluorescence lifetime of 3.49 ns. And the decipherment of conformers in protein is confined to the solution, and the existence of diverse Trp residue rotamers has also been independently proved through nuclear magnetic resonance.⁵⁸

As a result, we are not going to talk about the separate elements, but instead the average fluorescence lifetime has been used to receive a qualitative notion. It is

clearly visible from Table 2 that the mean fluorescence lifetimes of HSA decrease from 5.98 ns to 5.71 ns (hesperidin) and 5.56 ns (hesperetin) at different flavanones concentrations, demonstrating that the extinction of protein Trp residue fluorescence by flavanones is predominantly static mechanism, and this conclusion is wonderfully in harmony with the previous Stern-Volmer analysis. Also, it will need to be pointed out the multiexponential fluorescence decay behavior is ascribed to disparate conformations of the globular protein rather than an apportionment of dissimilar Trp residues in the biopolymer of one conformation. The conformational changes of protein presented in this section sort well with the molecular modeling results and this aspect will be annotated expressly by employing circular dichroism below.

Binding domain

As has been argued, both hesperidin and hesperetin have been shown to be located within subdomains IIA and IIIA by the aid of molecular docking and MD simulation. To proof these results, site-specific displacement experiments and guanidine hydrochloride induced denaturation of protein have been executed herein. Regarding the three-dimensional structure of HSA, there are two famous binding domains on this protein, that is Sudlow's site I and site II, as recounted above. Site I is known as the warfarin-azapropazone site, and formed as a pocket in subdomain IIA, the lone Trp residue of the protein in this region. The inside wall of the cavity is formed by hydrophobic side chains, whereas the entrance to the hole is surrounded by positively

charged residues.⁵⁹ The peculiar trait of this site is the emplacement of the ligand, which is a bulky heterocyclic anion with a negative charge localized in the middle of the molecule, and ligands binding in site I embrace azapropazone, diiodosalicylic acid, phenylbutazone and warfarin.⁶⁰

Site II corresponds to the aperture of subdomain IIIA, and is known as the indole-benzodiazepine site, which is nearly the same size as site I, the interior of the patch is composed by hydrophobic amino acid residues and the exterior cave attached two key amino acid residues, i.e. Arg-410 and Tyr-411.⁶¹ Ligands binding to site II are aromatic carboxylic acids with negatively charged acidic group at the end of the molecule, e.g. diazepam, flufenamic acid, ibuprofen and propofol. Subsequently Brodersen et al.⁶² unearthed that digitoxin binding one HSA is independent from Sudlow's site, and perch on what was nominated as site III. In the present study, the competitors used involved warfarin, a typical marker for site I, diazepam for site II, digitoxin for site III and hemin for domain I.

Based upon the equation (3), the affinity constants of HSA-hesperidin/hesperetin were plotted from raw fluorescence data and found to be $2.466/5.943 \times 10^4 \text{ M}^{-1}$, $0.3529/0.8162 \times 10^4 \text{ M}^{-1}$, $0.7812/2.821 \times 10^4 \text{ M}^{-1}$, $2.194/5.676 \times 10^4 \text{ M}^{-1}$ and $2.227/5.739 \times 10^4 \text{ M}^{-1}$ for blank (Fig. S3), warfarin, diazepam, digitoxin and hemin, respectively. These results signify doubtlessly that the bound HSA-flavanones complexes were evidently influenced by the addition of warfarin, and secondly the diazepam. In other words both hesperidin and hesperetin shares the identical site with warfarin (major) and diazepam (minor) in HSA, and this verdict does cohere with the

results of molecular modeling and is also in concert with the following data calculated from denaturation of protein.

Generally, protein has binding patches that complex with other ligands and such pockets are frequently produced by the folding of the amino acid chains that gives rise to the three-dimensional structure of the protein. Protein can also be denatured through exposure to some chemicals such as guanidine hydrochloride (GuHCl) or urea, and the process of denaturation includes the disruption and possible destruction of both the secondary and tertiary structures and thus protein function. In order to further confirm the binding location of flavanones, GuHCl evoked unfolding of protein experiments was conducted in this section.

According to the outcomes of Ahmad et al.,⁶³ GuHCl caused protein unfolding comes to pass in multiple steps. At 1.4 M GuHCl, only domain III is wholly unfolded, the existence of a molten globule-like intermediate state of domain III around 1.8 M GuHCl concentration and at 3.2 M GuHCl, domain I is departed from the domain II, and domain I is entirely unfolded whereas domain II is partly. This unfolding procedure has also been evidenced by Galantini et al.,⁶⁴ who utilized a small-angle X-ray scattering and light scattering techniques to examine the unfolding pathway of fatted and defatted HSA. In the current environment, samples of different concentrations of GuHCl were prepared by mixing various molar ratios of GuHCl stock solution and Tris-HCl buffer, pH=7.4. The final solution mixture was incubated with dissimilar GuHCl amounts for 12 h at room temperature before fluorescence emission determinations, the original fluorescence intensity in the presence of various

concentrations of GuHCl were treated with the equation (3), and the reaction constants were observed to be $1.592/2.537 \times 10^4 \text{ M}^{-1}$, $0.7381/1.814 \times 10^4 \text{ M}^{-1}$ and $0.3114/0.8565 \times 10^4 \text{ M}^{-1}$ at 1.4 M, 1.8 M and 3.2 M GuHCl for hesperidin and hesperetin, respectively.

Obviously, the reaction capacity was reduced by 35.44%/57.31% at 1.4 M GuHCl for hesperidin/hesperetin, whereas at 3.2 M GuHCl, the values lowered 87.37%/85.59%, respectively. This means that the unfolding of domain II and domain III has great impacts on the HSA-flavanones biointeractions, but the extension of domain III is clearly less than the protension of domain II on the association ability of protein with flavanones. Thus, the outcomes of protein denaturation provide another conclusive testimony for the identification of the location of flavanones on the globular protein, i.e. subdomain IIA was one of the principal binding domains for flavanones on HSA molecule, and the subdomain IIIA is unmistakably a secondary site.

Conformational stability

As we have seen, molecular modeling and time-resolved fluorescence denotes that maybe the conformation of HSA has been disturbed in the presence of hesperidin and hesperetin, as the orderly noncovalent bonds in the binding cavities were perturbed through the conjugation of flavanones. To verify the conformational changes of HSA, circular dichroism (CD) method have been used to measure the HSA-flavanones

adducts quantitatively, and the raw CD spectra of protein in the absence and presence of flavanones were displayed in Fig. 9, and secondary structure components computed based on CD data were also pooled in Table 3.

Fig. 9 here about

Table 3 here about

Markedly, the CD curves illustrated two negative bands in the far-UV CD region at roughly 208 nm and 222 nm, feature of a α -helical structure of globular protein. One believable explanation is that the negative peaks between 208 and 209 nm and 222 and 223 nm are both contributed by $\pi \rightarrow \pi^*$ and $n \rightarrow \pi^*$ transition of amide groups and are also affected by the geometries of the polypeptide backbones.⁶⁵ Furthermore, Table 3 indicates explicitly that free HSA contains 58.2% α -helix, 8.6% β -sheet, 11.1% turn and 22.1% random coil, upon complex with flavanones, decline of α -helix was detected from 58.2% (free HSA) to 46.6% (HSA-hesperidin) and 45.1% (HSA-hesperetin), whereas increase in β -sheet, turn and random coil from 8.6%, 11.1% and 22.1% (free HSA) to 11.2%, 14.8% and 27.4% (HSA-hesperidin) and 11.7%, 15.3% and 27.9% (HSA-hesperetin) at a molar ratio of protein to flavanones of 1 : 8. The decrease of α -helix with an elevation in the β -sheet, turn and random coil demonstrating that flavanones conjugated with amino acid residues of the polypeptide chain and resulting in the destabilization of the HSA structural state, i.e. some extent of protein disarrangement after flavanones complexation.^{66,67}

Additionally, Table 3 also insinuate that the structural alterations of HSA caused by hesperetin are higher than hesperidin, and the reason for this is probably that the

stronger affinity of hesperetin to HSA can arouse even more evident noncovalent bonds within the protein so as to accommodate the flavanone more tightly. Consequently, the information of CD results substantiate indirectly the stability of HSA-hesperidin is beneath the HSA-hesperetin, which gives a vigorous proof to the preceding outcomes of molecular modeling.

Conclusions

In short, the current scenario discussed clearly the biomolecular recognition processes of the naturally bioactive products – hesperidin and its aglycone hesperetin which belong to the typically *Rutaceae* family with the pivotal biomacromolecule HSA by using biophysical techniques such as molecular docking, MD simulation, fluorescence and CD spectra. These outcomes confirm credibly that (1) the recognition strength of hesperetin with the subdomains IIA and IIIA is somewhat larger than its glycoside hesperidin overall, although hesperetin has a smaller structure as a result of lack of the glycoside units. This indicates that the import of glycoside group might reduce the recognition ability between HSA and part flavanones, and then generate adverse impacts on the absorption, distribution and bioavailability of these natural chemicals *in vivo*. (2) The association capability of either hesperidin or hesperetin for the subdomain IIIA on HSA is obviously subordinate to the subdomain IIA, which may be related to the relatively evident differences in the molecular structures of flavanones and the flexibility of subdomains IIA and IIIA in HSA. These

contrasts would induce the disparities of protein conformational changes in the HSA-flavanone biointeractions.

The spectroscopic information further proves quantitatively the results of molecular modeling, several amino acid residues such as Trp-214 acted as a key role in the noncovalent interactions, and these reactions led to the decrease of protein structure particularly α -helix from 58.2% to 46.6% (hesperidin) and 45.1% (hesperetin) in order to lodge the flavanones more suitably. Because plant active components, e.g. flavanones have the remarkable medicinal activities, these research findings could not only assist to rational study the bioavailability of different flavanones, but contribute to the integrative comprehension of influences of the intrinsic properties such as flexibility of some crucial biopolymers for the pharmacological effects of active natural products in the human body, thereby applying the biological activities of these natural compounds to better promote human health.

Associated Content

Supporting Information

The protocol of time-resolved fluorescence, principles of fluorescence quenching, calculation of recognition ability, the location of flavanones in HSA, the extent of Trp residue quenching and molecular recognition capability plot for the HSA-flavanones.

Author Information

Corresponding Author

*E-mail: weipeng@cau.edu.cn, wpeng@qau.edu.cn. Phone/fax: +86-29-87092367.

Notes

The authors declare no competing financial interest.

Acknowledgements

We are extremely indebted to Professor Ulrich Kragh-Hansen of Department of Medical Biochemistry, University of Aarhus, for the invaluable gift of his doctoral dissertation. We are very grateful to Dr. John S. Wishnok of Department of Biological Engineering, Massachusetts Institute of Technology, for his salutary contribution in language refinement and manuscript melioration. We thank Professor Seung Bum Park of Department of Chemistry, Seoul National University, for his warm support during the manuscript processing. Thanks also go to the reviewers of this manuscript for their insightful and valuable suggestions.

Abbreviations Used

Ala, alanine; ANOVA, analysis of variance; Arg, arginine; CD, circular dichroism; Glu, glutamic acid; GuHCl, guanidine hydrochloride; HSA, albumin from human serum; IRF, instrument response function; Lys, lysine; MD simulation, molecular dynamics simulation; NPT, isothermal-isobaric; Phe, phenylalanine; PME, Particle Mesh Ewald; R, correlation coefficient; RMSD, Root-Mean-Square Deviation; RMSF, Root-Mean-Square Fluctuation; S.D., standard deviation; Thr, threonine; Tris, tris(hydroxymethyl)aminomethane; Trp, tryptophan; Tyr, tyrosine; Val, valine.

References

1. J. A. Ross and C. M. Kasum, *Annu. Rev. Nutr.*, 2002, **22**, 19-34.
2. F. D. Meo, V. Lemaur, J. Cornil, R. Lazzaroni, J.-L. Duroux, Y. Olivier and P. Trouillas, *J. Phys. Chem. A*, 2013, **117**, 2082-2092.
3. A. Crozier, I. B. Jaganath and M. N. Clifford, *Nat. Prod. Rep.*, 2009, **26**, 1001-1043.
4. B. S. Patil, G. K. Jayaprakasha, K. N. C. Murthy and A. Vikram, *J. Agric. Food Chem.*, 2009, **57**, 8142-8160.
5. R. J. Grayer and N. C. Veitch, in *Flavonoids: Chemistry, Biochemistry and Applications*, ed. Ø. M. Andersen and K. R. Markham, CRC Press, Taylor & Francis Group, Boca Raton, FL, 2006, pp. 917-1002.
6. C. Gardana, S. Guarnieri, P. Riso, P. Simonetti and M. Porrini, *Br. J. Nutr.*, 2007, **98**, 165-172.

7. S. Rusznyák and A. Szent-Györgyi, *Nature*, 1936, **138**, 27.
8. K. Kawaguchi, H. Maruyama, T. Kometani and Y. Kumazawa, *Planta Med.*, 2006, **72**, 477-479.
9. L. M. Loscalzo, T. T. Yow, C. Wasowski, M. Chebib and M. Marder, *Pharmacol. Biochem. Behav.*, 2011, **99**, 333-341.
10. J. Elavarasan, P. Velusamy, T. Ganesan, S. K. Ramakrishnan, D. Rajasekaran and K. Periandavan, *J. Pharm. Pharmacol.*, 2012, **64**, 1472-1482.
11. A. Garg, S. Garg, L. J. D. Zaneveld and A. K. Singla, *Phytother. Res.*, 2001, **15**, 655-669.
12. E. Tripoli, M. L. Guardia, S. Giammanco, D. D. Majo and M. Giammanco, *Food Chem.*, 2007, **104**, 466-479.
13. A. Soto-Vaca, A. Gutierrez, J. N. Losso, Z. M. Xu and J. W. Finley, *J. Agric. Food Chem.*, 2012, **60**, 6658-6677.
14. A. Chanet, D. Milenkovic, C. Manach, A. Mazur and C. Morand, *J. Agric. Food Chem.*, 2012, **60**, 8809-8822.
15. A. Gironés-Vilaplana, D. A. Moreno and C. García-Viguera, *Food Funct.*, 2014, **5**, 764-772.
16. A. Roohbakhsh, H. Parhiz, F. Soltani, R. Rezaee and M. Iranshahi, *Life Sci.*, 2014, **113**, 1-6.
17. J. Q. Silveira, T. B. Cesar, J. A. Manthey, E. A. Baldwin, J. H. Bai and S. Raithore, *J. Agric. Food Chem.*, 2014, **62**, 12576-12584.
18. B. Ameer, R. A. Weintraub, J. V. Johnson, R. A. Yost and R. L. Rouseff, *Clin.*

- Pharmacol. Ther.*, 1996, **60**, 34-40.
19. I. Demonty, Y. G. Lin, Y. E. M. P. Zebregs, M. A. Vermeer, H. C. M. van der Knaap, M. Jäkel and E. A. Trautwein, *J. Nutr.*, 2010, **140**, 1615-1620.
 20. M. Tomás-Navarro, F. Vallejo, E. Sentandreu, J. L. Navarro and F. A. Tomás-Barberán, *J. Agric. Food Chem.*, 2014, **62**, 24-27.
 21. P. A. Kroon, M. N. Clifford, A. Crozier, A. J. Day, J. L. Donovan, C. Manach and G. Williamson, *Am. J. Clin. Nutr.*, 2004, **80**, 15-21.
 22. O. Dangles, C. Dufour, C. Manach, C. Morand and C. Remesy, *Methods Enzymol.*, 2001, **335**, 319-333.
 23. M. Yamamoto, H. Jokura, K. Hashizume, H. Ominami, Y. Shibuya, A. Suzuki, T. Hase and A. Shimotoyodome, *Food Funct.*, 2013, **4**, 1346-1351.
 24. Z. Filip, K. Jan, S. Vendula, K. Z. Jana, M. Kamil and K. Kamil, *Expert Opin. Drug Metab. Toxicol.*, 2013, **9**, 943-954.
 25. D.-H. Tsai, F. W. DelRio, A. M. Keene, K. M. Tyner, R. I. MacCuspie, T. J. Cho, M. R. Zachariah and V. A. Hackley, *Langmuir*, 2011, **27**, 2464-2477.
 26. I. Vayá, V. Lhiaubet-Vallet, M. C. Jiménez and M. A. Miranda, *Chem. Soc. Rev.*, 2014, **43**, 4102-4122.
 27. N. A. Davies, R. Garcia, A. Proven and R. Jalan, in *Ascites, Hyponatremia and Hepatorenal Syndrome: Progress in Treatment*, ed. A. L. Gerbes, Karger Medical and Scientific Publishers, Basel, Switzerland, 2011, vol. 28, pp 40-51.
 28. X. M. He and D. C. Carter, *Nature*, 1992, **358**, 209-215.
 29. G. Sudlow, D. J. Birkett and D. N. Wade, *Mol. Pharmacol.*, 1975, **11**, 824-832.

30. F. Zsila, *Mol. Pharmaceutics*, 2013, **10**, 1668-1682.
31. C. F. Wong and J. A. McCammon, *Annu. Rev. Pharmacol. Toxicol.*, 2003, **43**, 31-45.
32. A. Perdih, M. Hrast, H. Barreteau, S. Gobec, G. Wolber and T. Solmajer, *J. Chem. Inf. Model.*, 2014, **54**, 1451-1466.
33. J.-S. Mandeville, E. Froehlich and H. A. Tajmir-Riahi, *J. Pharm. Biomed. Anal.*, 2009, **49**, 468-474.
34. M. K. Khan, N. Rakotomanomana, C. Dufour and O. Dangles, *Food Funct.*, 2011, **2**, 617-626.
35. D. Barreca, G. Laganà, G. Bruno, S. Magazù and E. Bellocco, *Biochimie*, 2013, **95**, 2042-2049.
36. F. Ding, J.-X. Diao, Y. Sun and Y. Sun, *J. Agric. Food Chem.*, 2012, **60**, 7218-7228.
37. O. H. Lowry, N. J. Rosebrough, A. L. Farr and R. J. Randall, *J. Biol. Chem.*, 1951, **193**, 265-275.
38. I. Petitpas, A. A. Bhattacharya, S. Twine, M. East and S. Curry, *J. Biol. Chem.*, 2001, **276**, 22804-22809.
39. D. van der Spoel, E. Lindahl, B. Hess, G. Groenhof, A. E. Mark and H. J. C. Berendsen, *J. Comput. Chem.*, 2005, **26**, 1701-1718.
40. C. Oostenbrink, A. Villa, A. E. Mark and W. F. van Gunsteren, *J. Comput. Chem.*, 2004, **25**, 1656-1676.
41. A. W. Schüttelkopf and D. M. F. van Aalten, *Acta Crystallogr. Sect. D: Biol.*

- Crystallogr.*, 2004, **60**, 1355-1363.
42. H. J. C. Berendsen, J. P. M. Postma, W. F. van Gunsteren, A. DiNola and J. R. Haak, *J. Chem. Phys.*, 1984, **81**, 3684-3690.
43. B. Hess, H. Bekker, H. J. C. Berendsen and J. G. E. M. Fraaije, *J. Comput. Chem.*, 1997, **18**, 1463-1472.
44. T. Darden, D. York and L. Pedersen, *J. Chem. Phys.*, 1993, **98**, 10089-10092.
45. J. A. Snyman, in *Practical Mathematical Optimization: An Introduction to Basic Optimization Theory and Classical and New Gradient-Based Algorithms*, Springer Science+Business Media, New York, NY, 2005, vol. 97, pp 33-150.
46. M. R. Hestenes and E. Stiefel, *J. Res. Natl. Bur. Stand.*, 1952, **49**, 409-436.
47. W. Humphrey, A. Dalke and K. Schulten, *J. Mol. Graph.*, 1996, **14**, 33-38.
48. N. Brooijmans and I. D. Kuntz, *Annu. Rev. Biophys. Biomol. Struct.*, 2003, **32**, 335-373.
49. B. Gipson, D. Hsu, L. E. Kaviraki and J.-C. Latombe, *Annu. Rev. Anal. Chem.*, 2012, **5**, 273-291.
50. R. O. Dror, R. M. Dirks, J. P. Grossman, H. F. Xu and D. E. Shaw, *Annu. Rev. Biophys.*, 2012, **41**, 429-452.
51. R. Hovius, P. Vallotton, T. Wohland and H. Vogel, *Trends Pharmacol. Sci.*, 2000, **21**, 266-273.
52. W. Gärtner, *ChemBioChem*, 2010, **11**, 1649-1652.
53. E. Froehlich, J. S. Mandeville, C. J. Jennings, R. Sedaghat-Herati and H. A. Tajmir-Riahi, *J. Phys. Chem. B*, 2009, **113**, 6986-6993.

54. M. Mansurova, J. Simon, S. Salzmann, C. M. Marian and W. Gärtner, *ChemBioChem*, 2013, **14**, 645-654.
55. F. Samari, B. Hemmateenejad, M. Shamsipur, M. Rashidi and H. Samouei, *Inorg. Chem.*, 2012, **51**, 3454-3464.
56. J. M. Beechem and L. Brand, *Annu. Rev. Biochem.*, 1985, **54**, 43-71.
57. J. A. Ross and D. M. Jameson, *Photochem. Photobiol. Sci.*, 2008, **7**, 1301-1312.
58. B. Dezube, C. M. Dobson and C. E. Teague, *J. Chem. Soc., Perkin Trans. 2*, 1981, **4**, 730-735.
59. T. Peters Jr., in *All about Albumin: Biochemistry, Genetics, and Medical Applications*, Academic Press, Elsevier Inc., San Diego, CA, 1995, pp 9-132.
60. J. Ghuman, P. A. Zunszain, I. Petitpas, A. A. Bhattacharya, M. Otagiri and S. Curry, *J. Mol. Biol.*, 2005, **353**, 38-52.
61. D. C. Carter and J. X. Ho, *Adv. Protein Chem.*, 1994, **45**, 153-203.
62. R. Brodersen, T. Sjödin and I. Sjöholm, *J. Biol. Chem.*, 1977, **252**, 5067-5072.
63. B. Ahmad, M. Z. Ahmed, S. K. Haq and R. H. Khan, *Biochim. Biophys. Acta – Proteins Proteomics*, 2005, **1750**, 93-102.
64. L. Galantini, C. Leggio and N. V. Pavel, *J. Phys. Chem. B*, 2008, **112**, 15460-15469.
65. N. J. Greenfield, *Nat. Protoc.*, 2006, **1**, 2876-2890.
66. P. Bourassa, S. Dubeau, G. M. Maharvi, A. H. Fauq, T. J. Thomas and H. A. Tajmir-Riahi, *Eur. J. Med. Chem.*, 2011, **46**, 4344-4353.
67. U. Katrahalli, V. K. A. Kalalbandi and J. Seetharamappa, *J. Pharm. Biomed. Anal.*,

2012, **59**, 102-108.

Figure Captions:

Fig. 1. Molecular structures of hesperidin (A) and hesperetin (B).

Fig. 2. The ribbon model of the albumin from human serum (HSA) resolved from X-ray diffraction crystallography (PDB: 1AO6) and subdivision of HSA into domain (I, II and III) and the subdomains (A and B) is designated. This diagram was made with PyMOL on the basis of the atomic coordinates available at the Brookhaven Protein Data Bank (<http://www.rcsb.org>).

Fig. 3. Molecular docking of hesperidin ((A) and (B)) and hesperetin ((C) and (D)) docked to HSA. The ball-and-stick model shows flavanones, colored as per the atoms and the key amino acid residues around flavanones have been displayed in stick model; green stick model exhibits hydrogen bonds between Lys-195, Arg-218, Arg-222, Arg-257, Ala-291 (A), Arg-410, Tyr-411, Glu-492, Thr-540 (B), Tyr-150, Lys-195, Lys-199, Arg-222, Arg-257, Ala-291 (C), and Arg-410, Lys-413, Lys-414, Glu-492, Val-493, Thr-540 (D) residues and flavanones; orange stick model indicates $T-\pi$ stacking between Trp-214 ((A) and (C)) residue and flavanones. (For interpretation of the references to color in this figure legend, the reader is referred to the web version of the article.)

Fig. 4. Calculated Root-Mean-Square Deviation (RMSD) for the backbone C_α atoms

of HSA and the flavanones from MD simulation at temperature of 298 K with respect to their docking results as a function of the simulation time. The pink and orange trajectories symbolize RMSD values for the backbone C_{α} atoms of HSA and the flavanones, respectively. (A): HSA-hesperidin (subdomain IIA); (B): HSA-hesperidin (subdomain IIIA); (C): HSA-hesperetin (subdomain IIA); and (D): HSA-hesperetin (subdomain IIIA).

Fig. 5. Superposition of the average conformations of MD simulation on the original conformations of molecular docking originating from the HSA-hesperidin ((A) and (B)) and the HSA-hesperetin ((C) and (D)) adducts. Protein manifested in surface colored in yellow (initial) and magenta (A), aquamarine (B), light green (C), and cyan (D) (average), respectively, and the original and average conformations of flavanones also denoted in yellow (initial) and light magenta (A), green (B), chartreuse (C), and skyblue (D) (average) carbon skeleton model. The crucial amino acid residues around flavanones have been expressed in stick model, and the marine (A), deep salmon (B), salmon (C), and orange (D) stick model conveys average conformations of different residues in HSA. (A): HSA-hesperidin (subdomain IIA); (B): HSA-hesperidin (subdomain IIIA); (C): HSA-hesperetin (subdomain IIA); and (D): HSA-hesperetin (subdomain IIIA).

Fig. 6. Root-Mean-Square Fluctuation (RMSF) of the backbone of each residue atomic positions for the flavanones situate within subdomains IIA (A) and IIIA (B) as

a function of the atom location along the polypeptide chain, respectively. (A): HSA-hesperidin (orange) and HSA-hesperetin (dark cyan); (B): HSA-hesperidin (pink) and HSA-hesperetin (olive).

Fig. 7. Fluorescence emission spectra of HSA with different amounts of hesperidin (A) and hesperetin (B) at pH = 7.4 and $T = 298$ K. (a)→(i): $c(\text{HSA}) = 1.0 \mu\text{M}$, $c(\text{flavanones}) = 0, 10, 20, 30, 40, 50, 60, 70$ and $80 \mu\text{M}$, (x): $80 \mu\text{M}$ flavanones solely.

Fig. 8. Stern-Volmer pattern recounting Trp residue quenching of HSA ($1.0 \mu\text{M}$) at pH = 7.4 and $T = 298$ K in the presence of various concentrations of flavanones. (■) Hesperidin, $y = 0.00504x + 0.9954$, $R = 0.9994$; (●) hesperetin, $y = 0.00665x + 0.9674$, $R = 0.9995$. Fluorescence emission intensity was examined at $\lambda_{\text{ex}} = 295$ nm, and the λ_{em} maximum read at 334 nm. All data were corrected for quencher fluorescence and each point was the mean of three individual experiments \pm S.D. ranging 0.3%–1.45%.

Fig. 9. Far-UV CD curves of HSA conjugates with hesperidin (A) and hesperetin (B) at pH = 7.4 and $T = 298$ K. (a)→(d): $5.0 \mu\text{M}$ HSA in the existence of 0 (black), 10 (red), 20 (green) and 40 (blue) μM flavanones. The cyan dashed line represents flavanones ($40 \mu\text{M}$) alone.

Table 1

Hydrogen bonds analyses from the calculations of molecular docking for HSA with flavanones

Protein-ligand systems	Donor	Acceptor	Distance (Å)
HSA (IIA)-hesperidin	Lys-195-NH ₃	tetrahydropyran ring (D)-OH	1.98
	Arg-218-NH ₂	tetrahydropyran ring (B)-OCH ₃	3.19
	Arg-218-NH ₂	tetrahydropyran ring (C)-O	3.02
	Arg-222-NH ₂	benzene ring (A)-O	2.21
	Arg-222-NH ₂	tetrahydropyran ring (D)-O	2.04
	Arg-257-NH	tetrahydropyran ring (E)-OH	2.55
	Arg-257-NH ₂	tetrahydropyran ring (E)-OH	3.07
	Ala-291-NH ₂	tetrahydropyran ring (E)-OH	2.78
HSA (IIIA)-hesperidin	Arg-410-NH ₂	benzene ring (A)-OH	2.23
	Tyr-411-OH	benzene ring (A)-OH	2.50
	tetrahydropyran ring (D)-OH	Glu-492-OH	2.56
	tetrahydropyran ring (D)-OH	Glu-492-OH	2.14
	Thr-540-NH ₂	tetrahydropyran ring (E)-OH	2.02
HSA (IIA)-hesperetin	Tyr-150-OH	tetrahydropyran ring (C)-OH	2.91
	Lys-195-NH ₂	benzene ring (B)-OCH ₃	3.42
	Lys-199-NH ₂	benzene ring (B)-OCH ₃	3.40
	Arg-222-NH ₂	benzene ring (B)-OH	1.99
	Arg-222-NH ₂	benzene ring (B)-OH	2.24
	Arg-257-NH ₂	tetrahydropyran ring (C)-O	2.86
	Arg-257-NH ₂	tetrahydropyran ring (C)-CO	2.16
	benzene ring (A)-OH	Arg-257-CO	2.13
benzene ring (B)-OH	Ala-291-CO	1.61	
HSA (IIIA)-hesperetin	benzene ring (A)-OH	Arg-410-CO	2.09
	benzene ring (A)-OH	Glu-492-COO	2.01
	benzene ring (A)-OH	Glu-492-COO	2.22
	Lys-413-NH ₂	tetrahydropyran ring (C)-O	3.41
	Lys-414-NH ₂	benzene ring (A)-OH	3.12
	Val-493-NH ₂	benzene ring (A)-OH	3.42
benzene ring (B)-OH	Thr-540-CO	2.08	

Table 2

Fluorescence lifetimes of HSA as a function of concentrations of flavanones

Samples	τ_1 (ns)	τ_2 (ns)	A_1	A_2	τ (ns)	χ^2
Free HSA	3.49	6.95	0.28	0.72	5.98	1.05
HSA+hesperidin (1 : 1)	3.11	7.09	0.27	0.73	6.02	1.13
HSA+hesperidin (1 : 2)	2.62	6.92	0.23	0.77	5.93	1.01
HSA+hesperidin (1 : 4)	2.34	6.57	0.19	0.81	5.77	1.05
HSA+hesperidin (1 : 8)	2.05	6.68	0.21	0.79	5.71	1.11
HSA+hesperetin (1 : 1)	3.29	7.18	0.31	0.69	5.97	1.01
HSA+hesperetin (1 : 2)	2.81	6.76	0.22	0.78	5.89	1.09
HSA+hesperetin (1 : 4)	2.42	7.14	0.34	0.66	5.54	1.17
HSA+hesperetin (1 : 8)	2.16	6.69	0.25	0.75	5.56	1.03

Table 3

Secondary structure ingredients of HSA conjugates with flavanones at pH=7.4 estimated by Jasco Spectra Manager II Software

Samples	Secondary structure components (%)			
	α -helix	β -sheet	Turn	Random
Free HSA	58.2	8.6	11.1	22.1
HSA + hesperidin (1 : 2)	55.3	9.3	12.2	23.2
HSA + hesperidin (1 : 4)	51.5	10.1	13.3	25.1
HSA + hesperidin (1 : 8)	46.6	11.2	14.8	27.4
HSA + hesperetin (1 : 2)	54.1	9.9	12.5	23.5
HSA + hesperetin (1 : 4)	50.2	10.8	13.6	25.4
HSA + hesperetin (1 : 8)	45.1	11.7	15.3	27.9

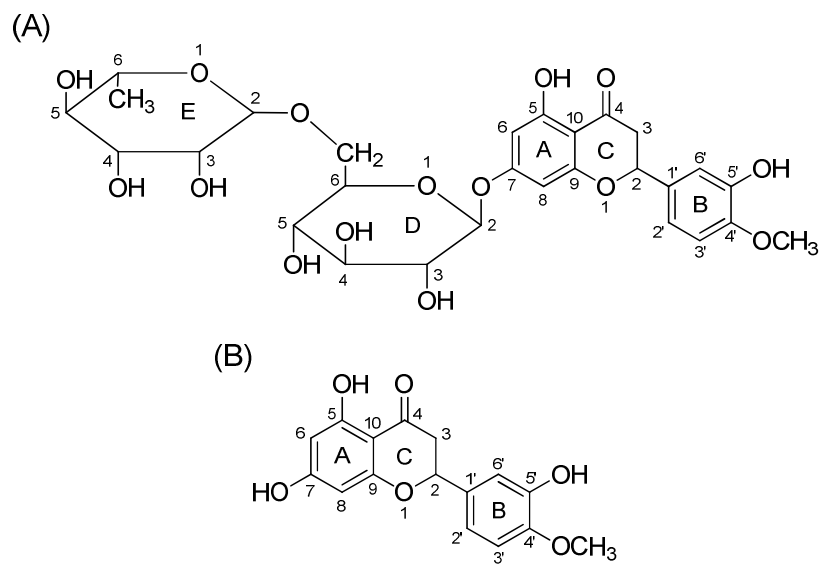


Fig. 1

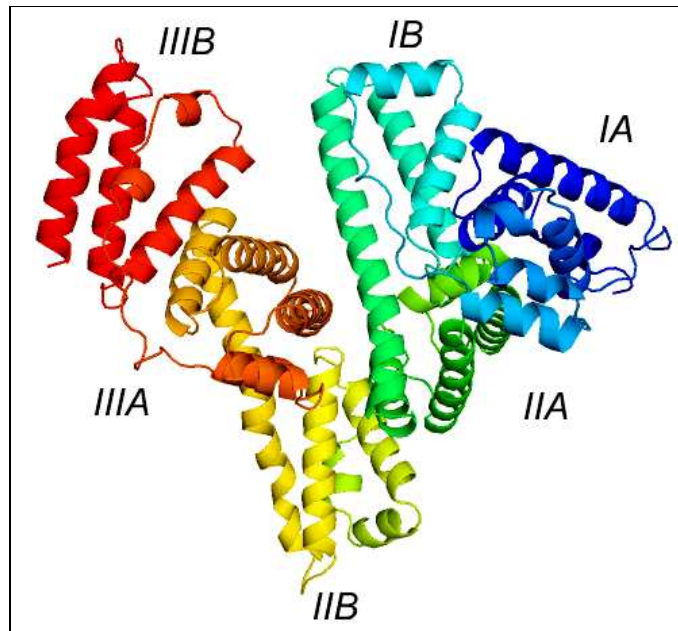


Fig. 2

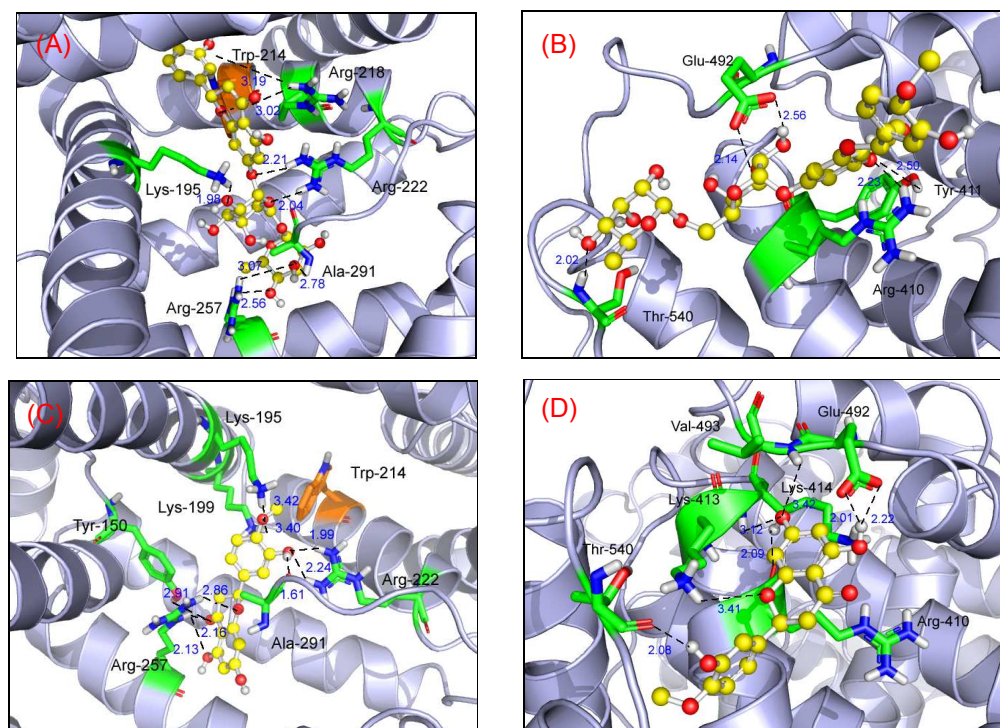


Fig. 3

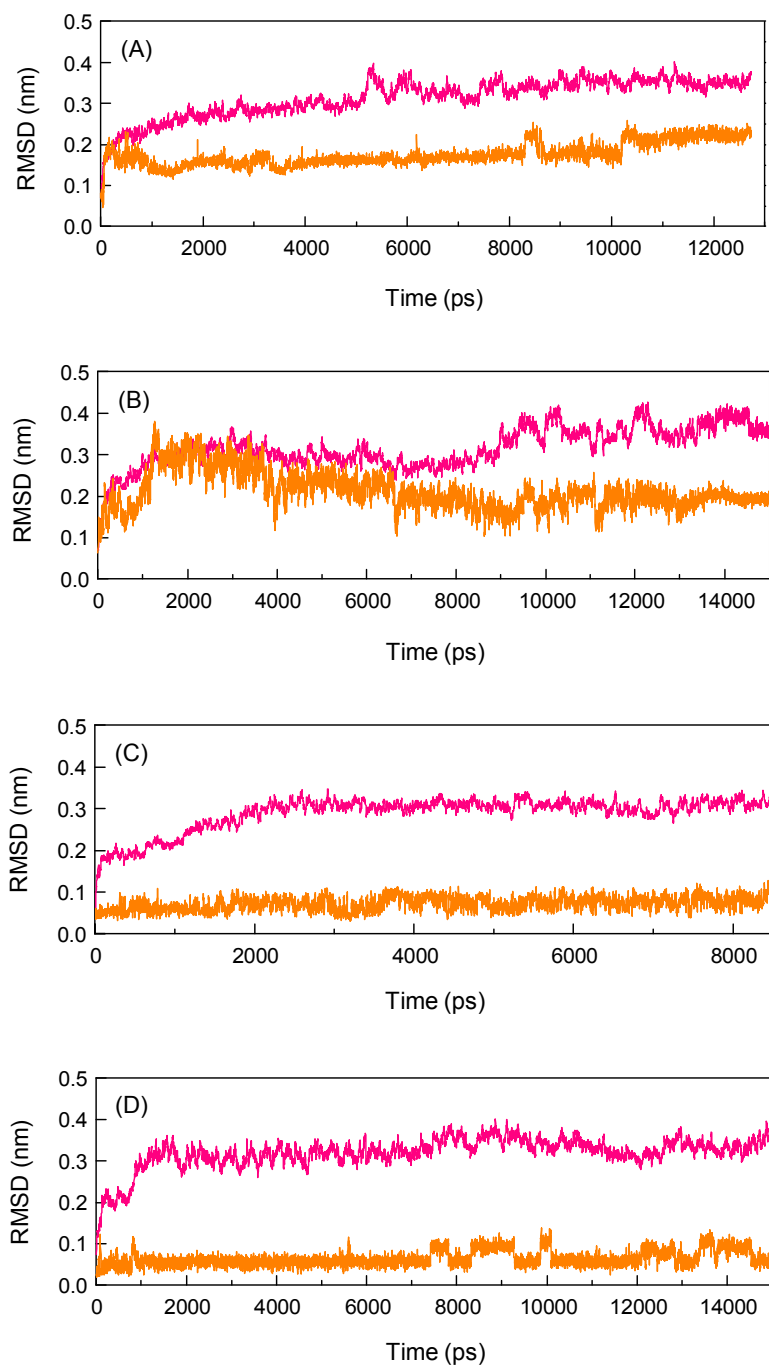


Fig. 4

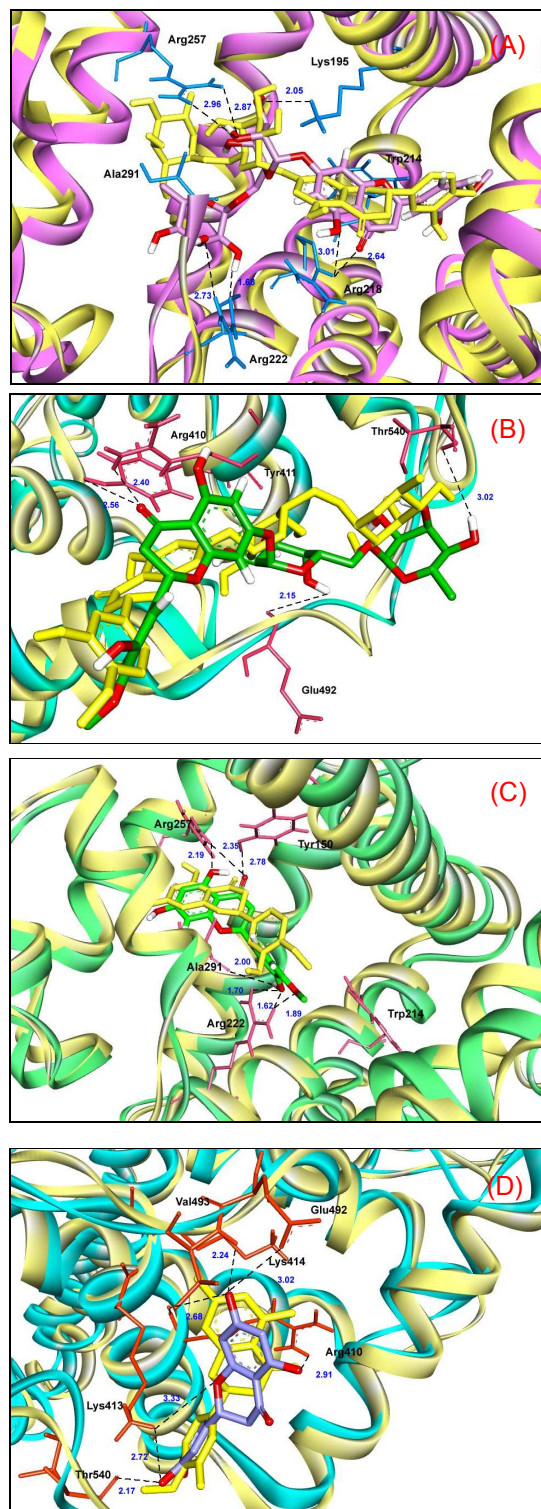


Fig. 5

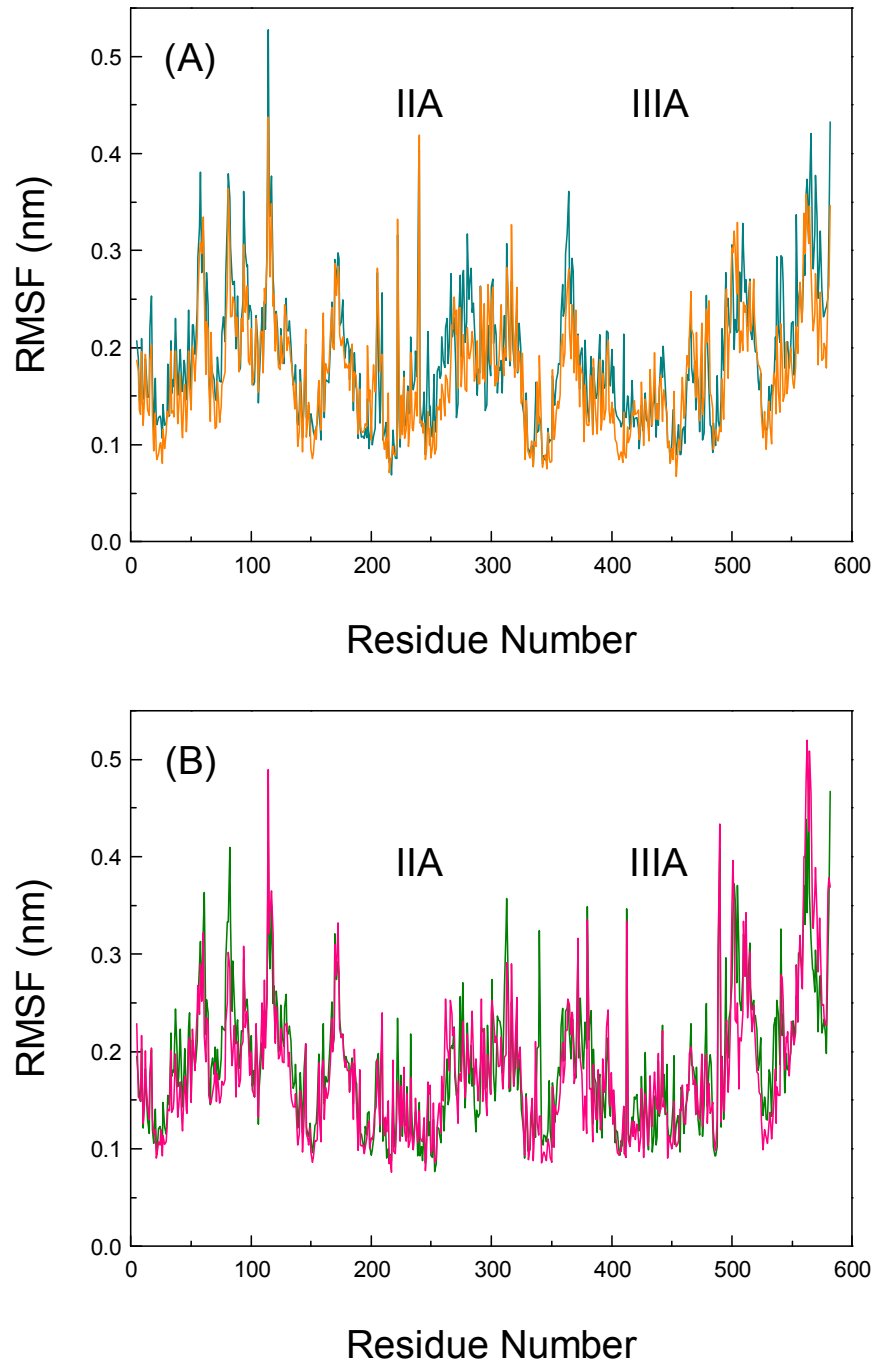


Fig. 6

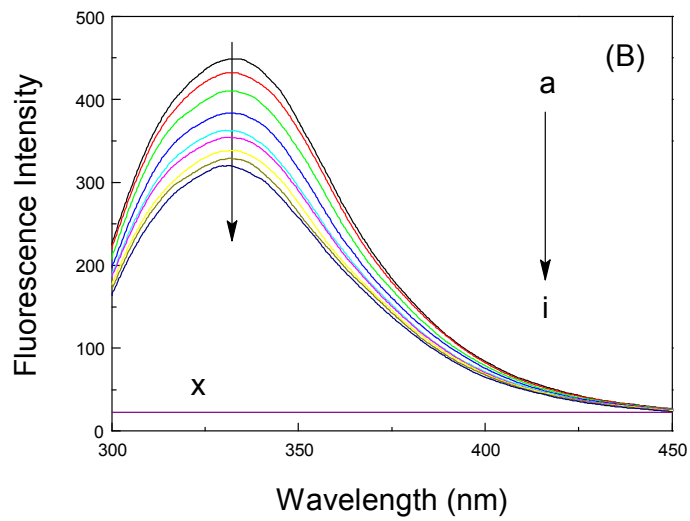
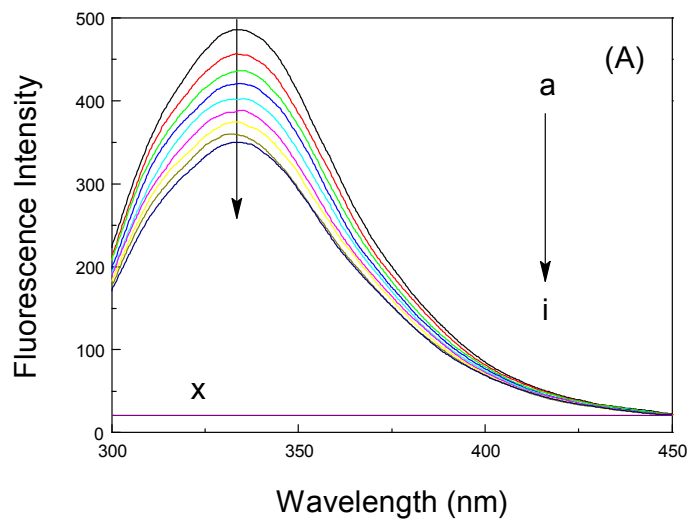


Fig. 7

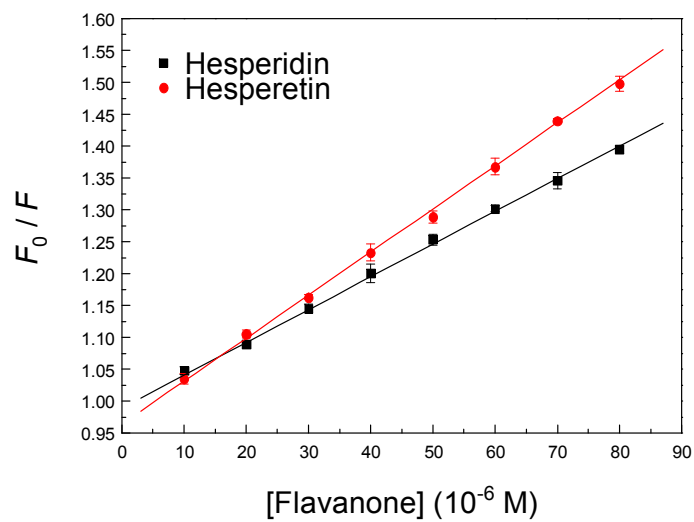


Fig. 8

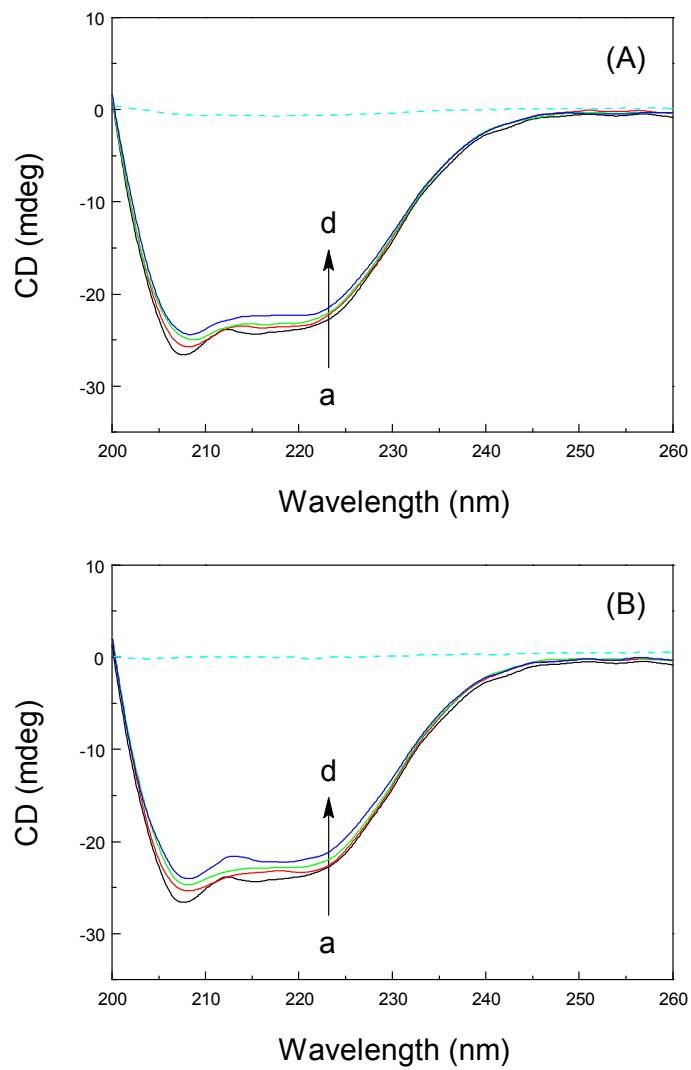


Fig. 9